MISP is a novel Plk1 substrate required for proper spindle orientation and mitotic progression

Mei Zhu,[1] Florian Settele,[1] Sachin Kotak,[2] Luis Sanchez-Pulido,[3] Lena Ehret,[1] Chris P. Ponting,[3] Pierre Gönczy,[2] and Ingrid Hoffmann[1]

[1]Cell Cycle Control and Carcinogenesis, German Cancer Research Center, DKFZ, D-69120 Heidelberg, Germany
[2]School of Life Sciences, Swiss Federal Institute of Technology (EPFL), Swiss Institute for Experimental Cancer Research (ISREC), CH-1015 Lausanne, Switzerland
[3]MRC Functional Genomics Unit, Department of Physiology, Anatomy and Genetics, University of Oxford, Oxford OX1 3QX, England, UK

Precise positioning of the mitotic spindle determines the correct cell division axis and is crucial for organism development. Spindle positioning is mediated through a cortical machinery by capturing astral microtubules, thereby generating pushing/pulling forces at the cell cortex. However, the molecular link between these two structures remains elusive. Here we describe a previously uncharacterized protein, MISP (C19orf21), as a substrate of Plk1 that is required for correct mitotic spindle positioning. MISP is an actin-associated protein throughout the cell cycle. MISP depletion led to an impaired metaphase-to-anaphase transition, which depended on phosphorylation by Plk1. Loss of MISP induced mitotic defects including spindle misorientation accompanied by shortened astral microtubules. Furthermore, we find that MISP formed a complex with and regulated the cortical distribution of the +TIP binding protein p150^{glued}, a subunit of the dynein–dynactin complex. We propose that Plk1 phosphorylates MISP, thus stabilizing cortical and astral microtubule attachments required for proper mitotic spindle positioning.

Introduction

The determination of the correct cell division axis is crucial for organism development and is mediated by the precise positioning of the mitotic spindle (Ahringer, 2003; Gönczy, 2008). External positioning signals are transmitted into the cell via the cell cortex (Théry et al., 2005; Toyoshima and Nishida, 2007) and relayed to the mitotic spindle through pulling forces acting on astral microtubules (MTs) attached to cortical structures (Grill et al., 2003). These cortical cues are spatially defined by retraction fibers modulating the positioning of actin regulators and therefore force generation (Théry et al., 2005; Fink et al., 2011). Moreover, astral MTs are engaged with these cortical structures through so-called +TIPs including adenomatous polyposis coli (APC), CLASPs, and the dynein–dynactin complex, which have been shown to regulate spindle orientation and positioning (O'Connell and Wang, 2000; Schuyler and Pellman, 2001; Rogers et al., 2002; Mimori-Kiyosue and Tsukita, 2003; Samora et al., 2011). The cortically localized dynein–dynactin complex is believed to provide pulling forces on astral MTs and is recruited by heterotrimeric G proteins/LGN/NuMA during spindle positioning in *Caenorhabditis elegans* embryos, *Drosophila*, and human cells (Du and Macara, 2004; Bowman et al., 2006; Siller et al., 2006; Couwenbergs et al., 2007; Nguyen-Ngoc et al., 2007; Woodard et al., 2010). However, the detailed mechanisms underlying the correct positioning and orientation of the mitotic spindle are still not fully understood and further investigation is needed to identify potential missing components involved in this process.

Polo-like kinase 1 (Plk1) is a major mitotic kinase important for many processes such as centrosome maturation, kinetochore–microtubule attachment, and furrow ingression (Petronczki et al., 2008). Plk1 binds to its interaction partners mainly through its Polo box domain (PBD), which is a phospho-peptide recognition motif that recognizes prephosphorylated, "primed" proteins (Elia et al., 2003a,b). This binding mechanism dynamically targets Plk1 to different subcellular localizations in mitosis like the centrosomes, kinetochores, spindle microtubules, and the central spindle (Petronczki et al., 2008;

M. Zhu and F. Settele contributed equally to this paper.

Correspondence to Ingrid Hoffmann: Ingrid.Hoffmann@dkfz.de

Abbreviations used in this paper: MISP, mitotic interactor and substrate of Plk1; MT, microtubule; NEB, nuclear envelope breakdown; PBD, Polo box domain; Plk1, Polo-like kinase 1; SAC, spindle activity checkpoint.

The Rockefeller University Press $30.00
J. Cell Biol. Vol. 200 No. 6 773–787
www.jcb.org/cgi/doi/10.1083/jcb.201207050

Johmura et al., 2011). Recently, it was shown that Plk1 phosphorylates Dvl2, a component of the Wnt signaling pathway, to regulate mitotic spindle orientation (Kikuchi et al., 2010). Moreover, spindle pole–localized Plk1 controls spindle positioning and orientation by regulating the binding between dynein–dynactin and its upstream cortical targeting factors NuMA and LGN (Kiyomitsu and Cheeseman, 2012).

Here, we report the identification of MISP, a previously uncharacterized actin-binding protein. We show that MISP is a mitotic phosphoprotein and substrate of Plk1. Phosphorylation of MISP by Plk1 is required for progression through mitosis and correct spindle orientation. Depletion of MISP impairs mitosis at the metaphase-to-anaphase transition with fragmented centrosomes, scattered chromosomes, and misoriented, rocking spindles. Furthermore, interference with MISP function causes a severe diminution of astral MTs. We find that MISP also associates with and negatively regulates the cortical distribution of $p150^{glued}$. Taken together, we describe that Plk1 targets a novel actin-binding protein involved in the regulation of spindle orientation and mitotic progression in human cells.

Results

Identification of MISP as a novel mitotic phosphoprotein and Plk1 substrate

To identify novel substrates and effectors of Plk1 during mitosis, we immunoprecipitated endogenous Plk1 from HeLa cells that were synchronized in late mitosis by nocodazole block and 1.5 h release, and subjected the immunoprecipitate to an in vitro kinase assay. Phosphorylated bands were analyzed by mass spectrometry resulting in the identification of C19orf21 (Fig. S1, A and B). Hereafter, we refer to C19orf21 as MISP (mitotic interactor and substrate of Plk1). MISP is a previously uncharacterized protein conserved among vertebrates and *Drosophila* with homologies to proteins of the AKAP family (Fig. S1 C). To analyze the function of MISP, rabbit polyclonal antibodies were raised against the full-length protein. In Western blots, the antibody recognized a major band at the expected molecular weight of ∼75 kD and a slower migrating band, which were largely reduced in MISP-depleted cells using two different siRNAs (Ol1 and Ol2; Fig. S1 D). To investigate whether MISP protein levels are regulated during the cell cycle, HeLa cells were synchronized with a double thymidine block at the G1/S boundary and released for different time points. Cell cycle progression was controlled by Western blot analysis of cell cycle marker proteins and monitored by FACS analysis. As shown in Fig. 1 A, MISP was only weakly expressed in G1 and S phases of synchronized HeLa cells, with increasing protein levels and slower migrating bands appearing stepwise in G2/M phases and persisting until the end of mitosis. The slower migrating form of MISP disappeared in response to λ-phosphatase treatment, indicating that MISP is a phosphoprotein (Fig. 1 B).

To assess the contribution of Plk1 function to the regulation of MISP during mitosis, we first sought to confirm the interaction between MISP and Plk1. As seen in Fig. 1 C, endogenous MISP was present in Plk1 immunoprecipitates. In addition, interactions between ectopically expressed Flag-MISP and Plk1 could also be detected in vivo (Fig. 1 D). Interestingly, Plk1 was found to bind to the highest phosphorylated form of MISP (Fig. 1 C). Plk1 is known to bind to substrates in a phospho-specific manner via its PBD (Elia et al., 2003a,b). To test this, we made use of a far Western blot assay (Neef et al., 2003). The GST-PBD of Plk1 was able to bind to the highest phosphorylated form of precipitated Flag-MISP in mitosis, while this interaction was weakened in asynchronous cells and abolished by λ-phosphatase treatment (Fig. 1 E, left). Moreover, a PBD mutant (W414F/H538A/K540M, FAM) deficient in phospho-peptide binding (Elia et al., 2003a,b) attenuated the ability to interact with Flag-MISP (Fig. 1 E, right; and Fig. S1 E). Then, the interaction of MISP with Plk1 was mapped in a GST pull-down assay. Different C-terminal truncations of Flag-MISP were generated and incubated with GST-Plk1 or Plk1 PBD. We found that the last 179 amino acids (aa 501–679) of the C-terminal MISP domain are required for binding to Plk1 and Plk1 PBD (Fig. S1, F and G; and unpublished data). Interestingly, the C-terminal domain is the most conserved part in MISP among different orthologues (Fig. S1 C).

To verify whether MISP is a substrate of Plk1, in vitro kinase assays with recombinant GST-MISP and His-Plk1 were performed in the presence or absence of the Plk1 inhibitor BI2536. As shown in Fig. 2 A, a strong phosphorylation of GST-MISP by Plk1 was detected and was weakened in the presence of BI2536. Furthermore, interference with Plk1 activity in mitosis by siRNA-mediated depletion led to a pronounced reduction of MISP phosphorylations (Fig. 2 B). Taken together, we identified MISP as a novel substrate and interaction partner of Plk1 in mitosis.

Cdk1 is an important mitotic kinase and was shown to be one of the major priming kinases for Plk1 binding. Thus, we attempted to detect an interaction between MISP and Cdk1. Endogenous Cdk1–cyclin B complexes interacted with endogenous MISP in mitotic HeLa cells (Fig. S2 A). Interestingly, Cdk1 interacted preferentially with a weakly phosphorylated, faster migrating form of MISP, hinting at a potential role of Cdk1 as the priming kinase for Plk1 phosphorylation. As expected, Cdk1 strongly phosphorylated GST-MISP in vitro and the phosphorylation was abolished in the presence of the Cdk inhibitor roscovitine (Fig. S2 B). The strong phosphorylation by Cdk1 led to an upshift of GST-MISP in the Coomassie gel reminiscent of mitotic MISP (unpublished data).

We next determined the potential phosphorylation sites of both kinases on MISP by mass spectrometry analysis after in vitro phosphorylation. Six potential sites for Plk1 and nine potential sites for Cdk1 were identified on MISP (Fig. S2 C). Mutations of the respective S/T residues to nonphosphorylatable alanines (9AC for Cdk1 and 7AP for Plk1) reduced the phosphorylation of GST-MISP by Plk1 (Fig. 2 C) and significantly abolished Cdk1 phosphorylation (Fig. 2 D). Moreover, ectopic expression of GFP-tagged versions of MISP revealed an accelerated electrophoretic mobility for both mutants in nocodazole-arrested HeLa cells (Fig. S2 D). Importantly, the PBD of Plk1 was unable to bind to the precipitated Flag-MISP 9AC mutant while it still bound to Flag-MISP WT and 7AP mutant (Fig. 2 E). Thus, Plk1 binds to MISP in mitosis through priming phosphorylation by Cdk1.

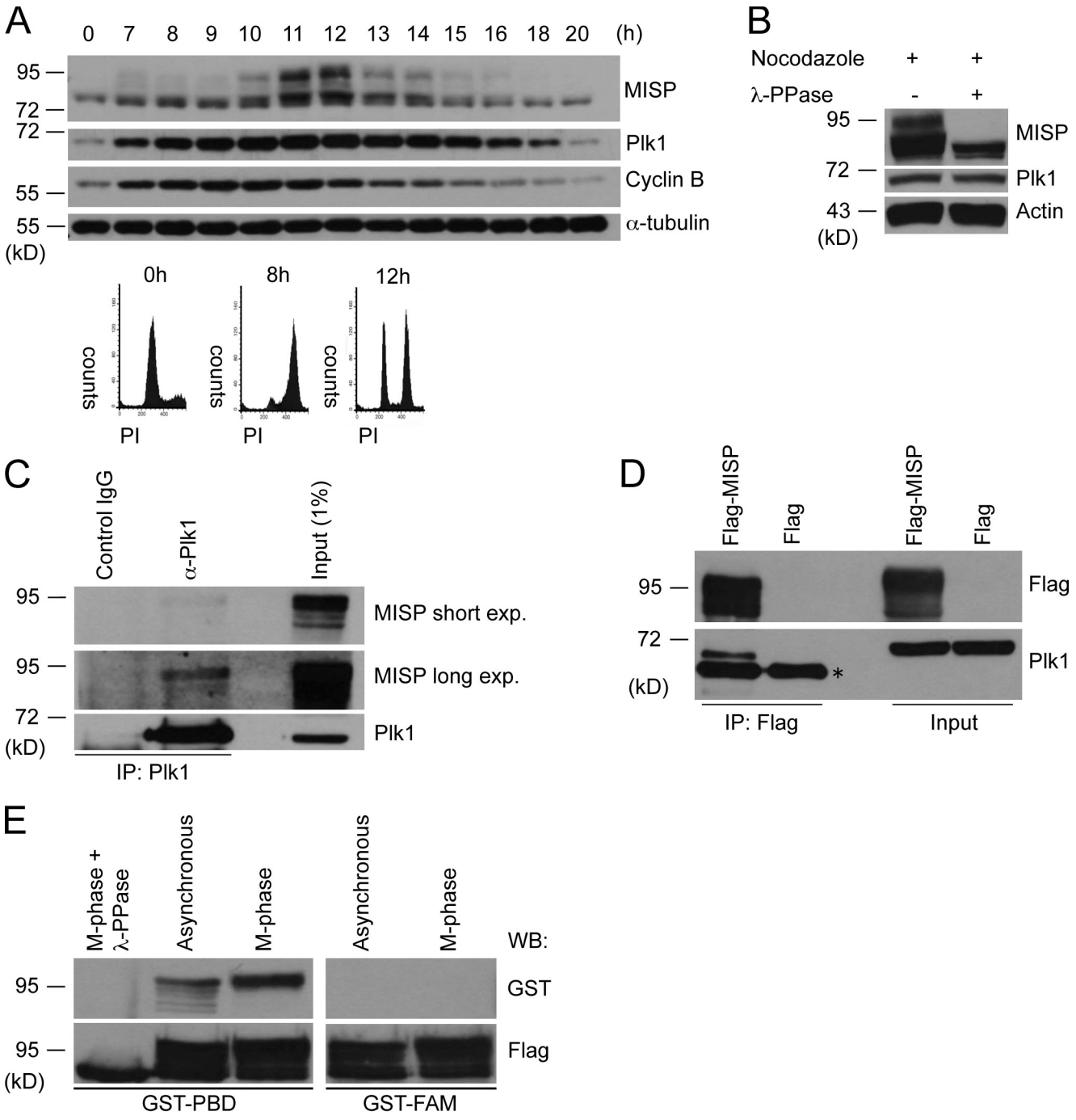

Figure 1. **MISP is a mitotic phosphoprotein and interacts with Plk1.** (A) HeLa cells were synchronized at the G1/S transition by a double thymidine block/release. Samples were analyzed by Western blot with depicted antibodies. FACS analyses of the DNA content by propidium iodide (PI) staining from indicated time points were performed. The experiment was repeated three times. (B) Nocodazole-blocked HeLa cells analyzed with indicated antibodies, with and without λ-phosphatase (λ-PPase) treatment. (C) Plk1 immunoprecipitated from mitotic HeLa cells was analyzed by Western blot with indicated antibodies. (D) HeLa cells were transfected with Flag or Flag-MISP and arrested in metaphase. Immunoprecipitation was performed using Flag M2 antibodies and were analyzed with indicated antibodies. Asterisk indicates IgGs. (E) Flag-MISP was overexpressed and immunoprecipitated from HeLa cells that were either untreated or arrested in mitosis. Far Western blot (FWB) analysis was performed using GST-PBD of Plk1 and GST-Plk1 Polo box mutant (FAM) and probed by Western blot. Mitotic lysates were additionally treated with λ-PPase.

MISP is an actin-binding protein that regulates the metaphase-to-anaphase transition

Next, we determined the subcellular localization of MISP during the cell cycle. MISP was found to be predominantly localized to cortical actin structures during interphase and mitosis as shown by immunofluorescence staining with MISP antibodies and phalloidin (Fig. 3 A). We also observed a partial colocalization of MISP with cytoplasmic actin filaments. A clear colocalization with actin filaments was observed upon overexpression of MISP in HeLa (Fig. S2 E) or RPE-1 cells (not depicted). MISP WT and the phospho-mutants (6DP, 7AP, 9AC) showed

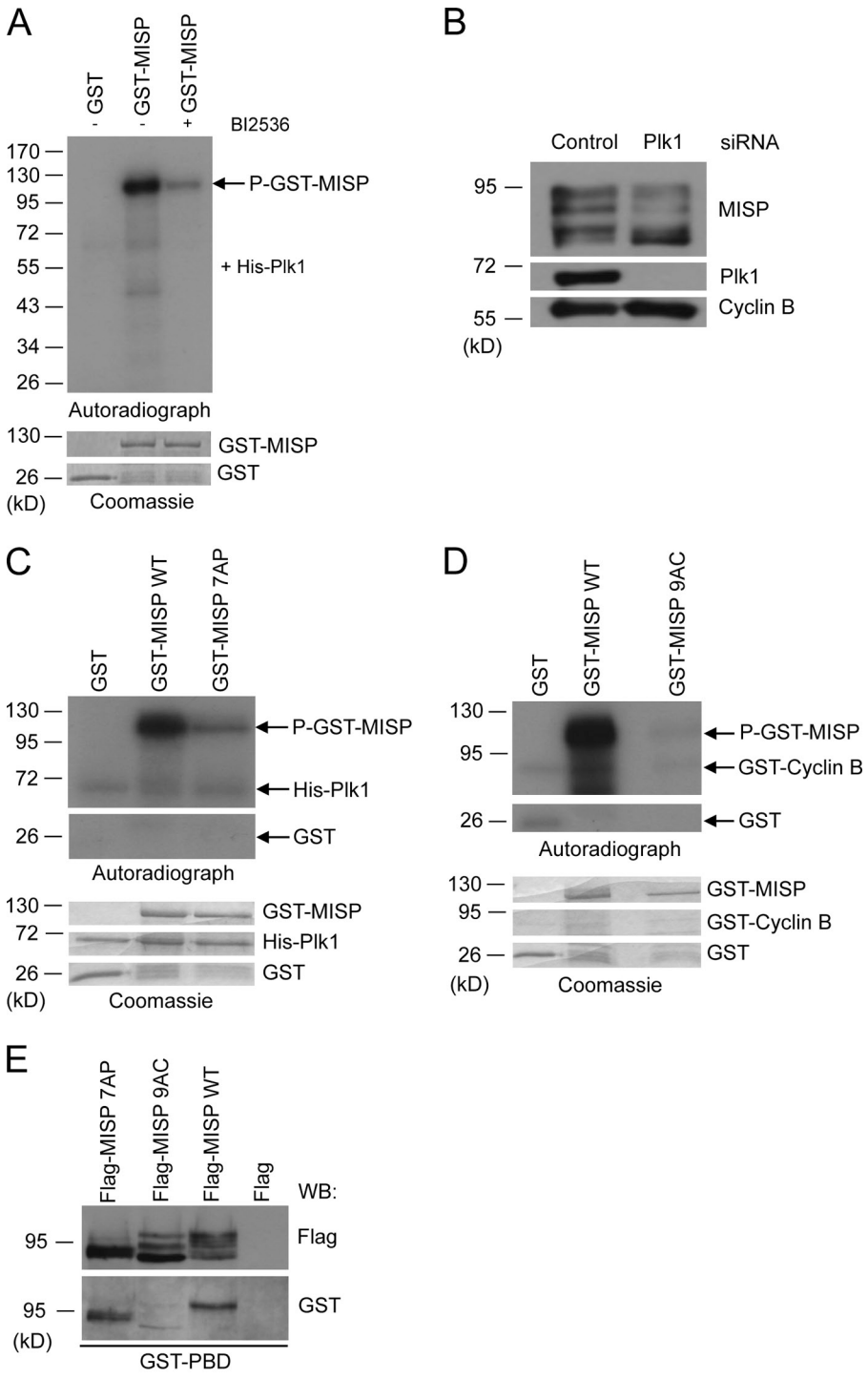

Figure 2. **Plk1 and Cdk1 regulate MISP phosphorylation.** (A) GST-MISP or GST was incubated with His-Plk1 and γ-[^{32}P]ATP (±100 nM of the Plk1 inhibitor BI2536) and analyzed by autoradiography. Coomassie staining shows equal loading. P-GST-MISP, phosphorylated GST-MISP. (B) HeLa cells were transfected with Plk1 or control siRNA for 36 h followed by 16 h of nocodazole treatment. Western blot analysis was performed with indicated antibodies. Cyclin B, loading control. (C) GST-MISP wild type (WT), 7AP mutant, or GST was incubated with His-Plk1 in the presence of γ-[^{32}P]ATP followed by autoradiography. Equal loading is shown by Coomassie staining. (D) GST-MISP WT, 9AC mutant, or GST was incubated with GST-cyclin B/His-Cdk1 in the presence of γ-[^{32}P]ATP followed by autoradiography. Equal loading is shown by Coomassie staining. (E) Flag-MISP WT/7AP/9AC or Flag alone was overexpressed and immunoprecipitated from mitotic HeLa cells. Far Western blot was performed using GST-Plk1 PBD and analyzed with indicated antibodies.

a similar cortical localization in mitotic cells (Fig. S2 F). We were not able to detect an obvious colocalization of MISP with the mitotic spindle (Fig. S3 A) or with Plk1 (Fig. S3 B), although it was found in the mitotic spindle phosphoproteome of Plk1 (Santamaria et al., 2011). We propose that the cytoplasmic part of MISP associates with Plk1 in vivo. MISP's cortical localization was disrupted by depolymerization of the actin network in response to cytochalasin D (Cyto. D) treatment (Figs. 3 B and S2 E) or siRNA-mediated depletion (Fig. S3 C), pointing to a specific localization of MISP at the cell cortex. We then set out to identify the potential of MISP to bind to actin filaments using an actin cosedimentation assay. We were able to detect substantial cosedimentation of GST-MISP with polymerized actin (F-actin; Fig. 3 C). Thus, MISP is an actin-associated protein.

To study the role of MISP during the cell cycle, we depleted endogenous MISP with Ol1 or Ol2. MISP depletion led to a marked increase in the number of mitotically rounded up cells (unpublished data). To confirm this observation, we made use of the mitotic marker p-Ser10 Histone H3 (p-Ser10 H3). We observed a three- to fivefold increase in the mitotic index evaluated by p-Ser10 H3 staining (Fig. 4, A and B) after MISP siRNA

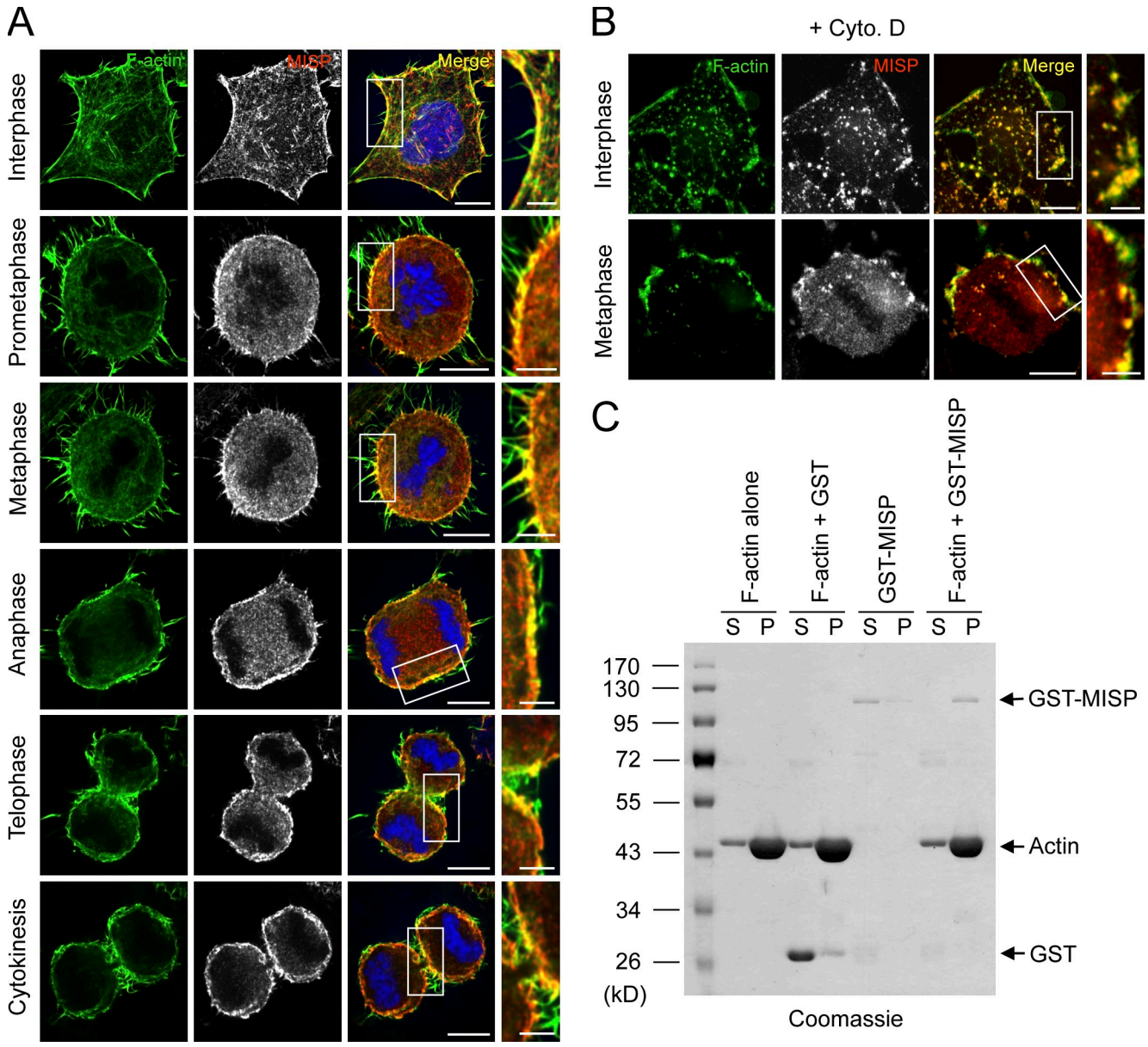

Figure 3. **MISP is an actin-associated protein.** (A) Localization of MISP (gray; red in merge) in interphase and different indicated mitotic stages of HeLa cells was shown by costaining with MISP antibody, Atto 488 phalloidin (green), and Hoechst 33342 (blue). Bars, 10 µm. Insets showed higher magnification of the framed regions. Bars, 5 µm. (B) HeLa cells were incubated with 2 µM of the actin-depolymerizing agent cytochalasin D (Cyto. D) for 10 min and analyzed by immunofluorescence. MISP, gray; red in merge; Atto 488 phalloidin, green. Bars, 10 µm. Insets showed higher magnification of the framed regions. Bars, 5 µm. (C) Actin cosedimentation assay with polymerized nonmuscle β-actin and GST-MISP or GST control. P, pellet; S, supernatant.

treatment. To ensure that this phenotype is not due to off-target effects, we performed a rescue experiment by generating an siRNA (Ol2)-resistant version of GFP-MISP that was coexpressed during siRNA-mediated depletion of endogenous MISP. GFP-MISP was able to reduce the mitotic index nearly back to control levels, which was not the case upon expression of the GFP control (Fig. S3, D and E). We next used time-lapse video microscopy to confirm the effect of MISP ablation and gain further insight into mitotic progression in real time. MISP was depleted in HeLa cells stably expressing GFP-α-tubulin/RFP-H2B or GFP-H2B and cells were monitored for 8–12 h after 24 h or 28 h of siRNA transfection. After MISP knockdown, around half of the mitotic cells entered anaphase and completed cytokinesis during the monitored period with an average time of 247 min from nuclear envelope breakdown (NEB) to anaphase transition (Videos 1 and 2) compared with 42 min (Video 3) in control cells (Fig. 4, C and D); the remainder ended with scattered chromosomes or cell death. After NEB, both control- and MISP-depleted cells exhibited bipolar spindle assembly; over 80% of MISP-depleted cells properly aligned their chromosomes during early mitosis, although some cells showed a slight delay compared with the control (Fig. 4, C and E; Videos 1–5). While control cells progressed to anaphase immediately after metaphase chromosome alignment, MISP-depleted cells were arrested with rocking and flipping spindles in metaphase in which the entire spindle oscillated within the cell for several

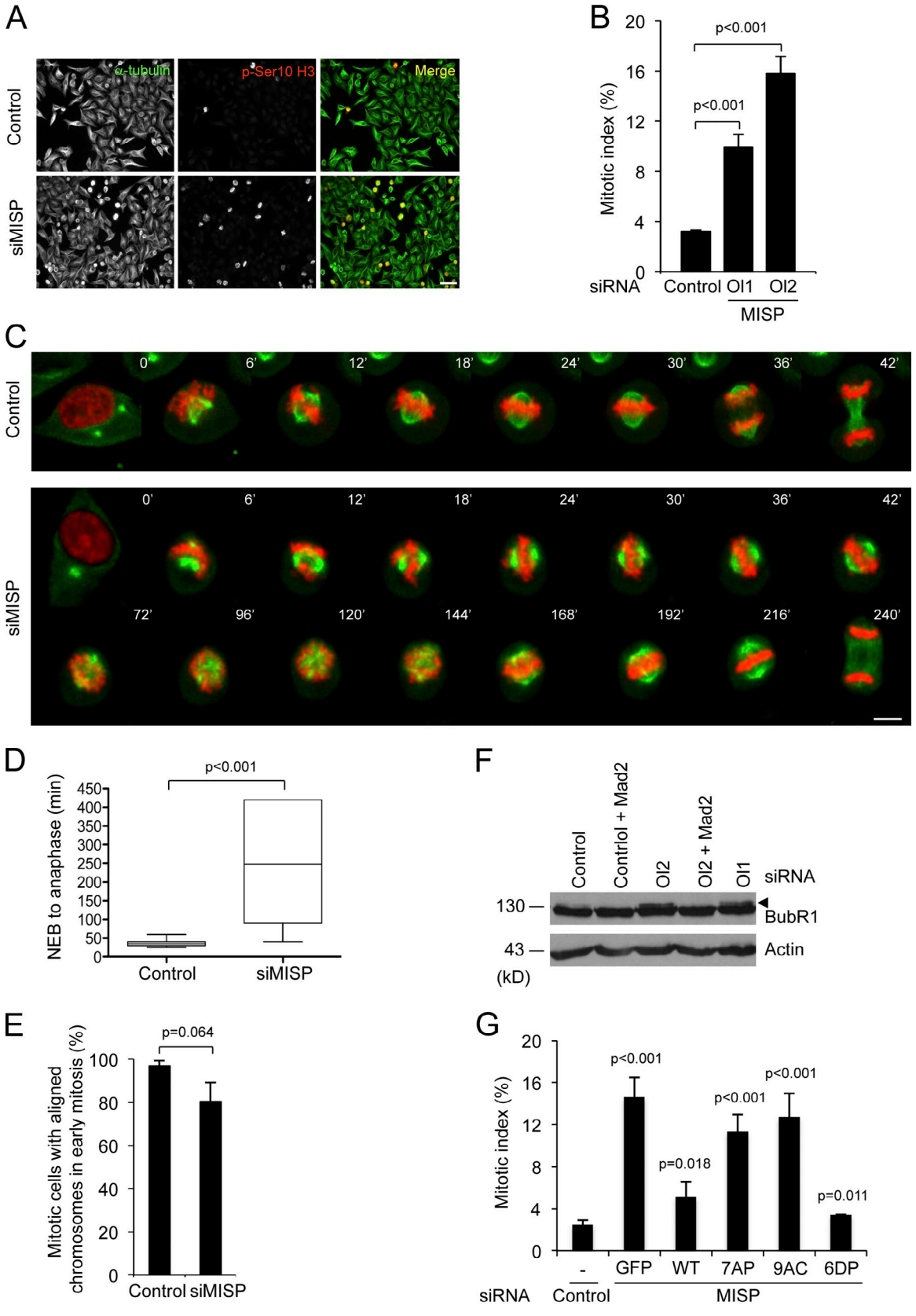

Figure 4. **Depletion of MISP impairs the metaphase-to-anaphase transition.** (A) Asynchronous HeLa cells were stained for p-Ser10 H3 (red) and α-tubulin (green) 48 h after control or MISP Ol2 siRNA treatment. Bar, 50 µm. (B) Quantification of the mitotic index in HeLa cells transfected with control or MISP siRNA (Ol1/Ol2) by evaluating p-Ser10 H3 staining. Results represent the mean of three different experiments (n = 200 cells per experiment). (C) HeLa cells stably expressing GFP-α-tubulin/RFP-H2B were transfected with control or MISP Ol2 for 24 h followed by live-cell imaging for 8 h. Frame series of movies of control and MISP knockdown cells with continuous time points (minute) are shown. Bar, 10 µm. (D) Box plot of C displaying the time from NEB to anaphase;

hours. The cortical integrity of most MISP-depleted cells remained intact, as visualized by phase-contrast imaging shown in Video 4 and by actin staining in fixed cells (Fig. S3 C).

The spindle assembly checkpoint (SAC) is a control mechanism that arrests cells with spindle defects or defective kinetochore–microtubule attachments at the metaphase-to-anaphase transition (Musacchio and Salmon, 2007). To investigate the activation state of the SAC after MISP depletion, we performed immunofluorescence analysis of fixed HeLa cells with an antibody against BubR1, a well-known marker of an active SAC. We detected clear BubR1 staining on kinetochores of cells with misaligned chromosomes, and observed a weak localization of BubR1 on kinetochores of cells with aligned chromosomes (Fig. S3 F, middle and bottom panels, respectively). We also detected increased phosphorylation of BubR1 after MISP depletion by Western blot (Fig. 4 F), indicating an active SAC (Mao et al., 2003). The remaining BubR1 signal upon MISP depletion prevents SAC satisfaction, thereby leading to a delay in the metaphase-to-anaphase transition. Furthermore, co-depletion of another core SAC protein, Mad2, together with MISP completely abolished the arrest in mitosis (Fig. 4 F; and Fig. S3, G and H). Thus, the arrest in metaphase as observed in response to MISP depletion is mediated by the SAC.

As MISP is highly phosphorylated during mitosis by Plk1 and Cdk1, we asked whether phosphorylation contributes to the function of MISP in regulating mitotic progression. We depleted endogenous MISP from HeLa cells and coexpressed GFP-tagged siRNA-resistant versions of MISP including WT, 7AP, 9AC, and 6DP (phospho-mimicking aspartic acid mutant of MISP for Plk1; Fig. S3 I). We found that both nonphosphorylatable mutants of MISP (7AP and 9AC) for Plk1 and Cdk1 were not able to rescue the observed mitotic arrest, whereas expression of the WT and the 6DP mutants successfully reduced the mitotic index nearly back to control levels (Fig. 4 G). From these data, we conclude that phosphorylation of MISP by Plk1 is required for its function in regulating the metaphase-to-anaphase transition.

Loss of MISP leads to spindle misorientation

As MISP knockdown delays anaphase entry, we set out to further analyze the effects of MISP depletion in mitotic cells in more detail. Close inspection of the mitotic spindle stained for α-tubulin and the centrosomal marker γ-tubulin in MISP-depleted cells revealed a marked increase in several mitotic defects such as chromosome misalignment, spindle tilt, disrupted spindle poles, and movement of the spindle out of the cell center to the cortex, with the majority of the cells showing one or a combination of the described defects (Fig. 5, A and B). The disruption of the spindle poles was further confirmed by inspection of another centrosomal marker, pericentrin (Fig. S4 A), and the centriolar marker Cep135 (Fig. S4 B). The observed multiple centrosome dots were not caused by centrosome overduplication, as just four centrioles were detected in MISP-depleted mitotic cells based on Cep135 staining. As we did not observe obvious disrupted spindle poles (Videos 1 and 2) and chromosome congression defects (Videos 1, 2, and 4) during early mitosis in MISP-depleted cells by live-cell imaging, we speculate that centrosome splitting and chromosome misalignment after MISP knockdown may be caused by a long-term metaphase arrest-induced "cohesion fatigue", which leads to sister chromatid separation followed by centriole disengagement and chromosome scattering (Daum et al., 2011; Stevens et al., 2011). To test this, we silenced the active SAC by co-depletion of Mad2 together with MISP. The percentage of metaphase cells with disrupted poles after Mad2 co-depletion was dramatically decreased compared with MISP knockdown alone (Fig. S4 C), pointing to an indirect role of MISP in centrosome splitting. The majority of MISP-depleted cells properly aligned chromosomes during early mitosis (Fig. 4 E). We propose that the chromosome misalignment, however, occurred afterward as shown in Video 4, and seemed also to be a secondary effect of prolonged metaphase arrest caused by uncoordinated cohesion loss. The SAC is then efficiently re-activated to maintain the scattered state of chromosomes (Stevens et al., 2011). Additionally, the split spindle poles in MISP knockdown cells had similar spindle microtubule nucleation activity as in control cells, validated by a microtubule regrowth assay (Fig. S4 D).

To characterize the observed spindle tilt more closely, the orientation of the mitotic spindle was determined in MISP-depleted HeLa cells grown on fibronectin-coated coverslips in relation to the substratum by confocal microscopy of the spindle and the spindle poles (Fig. 5 C). Inspection of the spindle poles revealed that in MISP-depleted cells, 29 ± 7% of the cells showed a spindle angle α of more than 20° as compared with 5 ± 7% in control cells (Fig. 5 D). The average spindle rotation increased to 14.2° in MISP-depleted cells from 8.6° in control cells (Fig. S4 E). To rule out the possibility that spindle misorientation in MISP-depleted cells is a consequence of an extended metaphase block, we arrested cells in metaphase in the presence of MG132 and analyzed spindle angles in control and MISP siRNA-treated cells as described in Fig. 5, C and D. Similar as observed before by live-cell imaging (Toyoshima et al., 2007; Chan et al., 2009), a short-time prolonged metaphase arrest by MG132 treatment did not markedly rotate the spindle along z-axis and attenuate the observed effect on spindle orientation after MISP knockdown (Fig. S4 F). Furthermore, down-regulation of CENP-E required for chromosome alignment leads to delayed metaphase-to-anaphase transition but without having an obvious effect on spindle orientation (Figs. 5 E

n = 20 cells each from three independent experiments. (E) Percentage of mitotic cells with aligned chromosomes during early mitosis in control and MISP siRNA-treated cells evaluated by live-cell imaging (*n* = 100 cells from two independent experiments). (F) HeLa cells were treated with control or MISP siRNAs with and without additional depletion of Mad2 for 48 h. Samples were analyzed by Western blot. Arrowhead indicates phosphorylated BubR1 with retarded electrophoretic mobility. (G) HeLa cells transiently transfected with GFP alone or siRNA-resistant versions of GFP-MISP WT/7AP/9AC/6DP were treated with MISP or control siRNA for 48 h. The mitotic index was evaluated (*n* = 200 cells) by p-Ser10 H3 staining, respectively from three independent experiments. Error bars in D, E, and G represent SD. Student's *t* test was used to calculate p-value for comparison of control- and MISP-depleted samples.

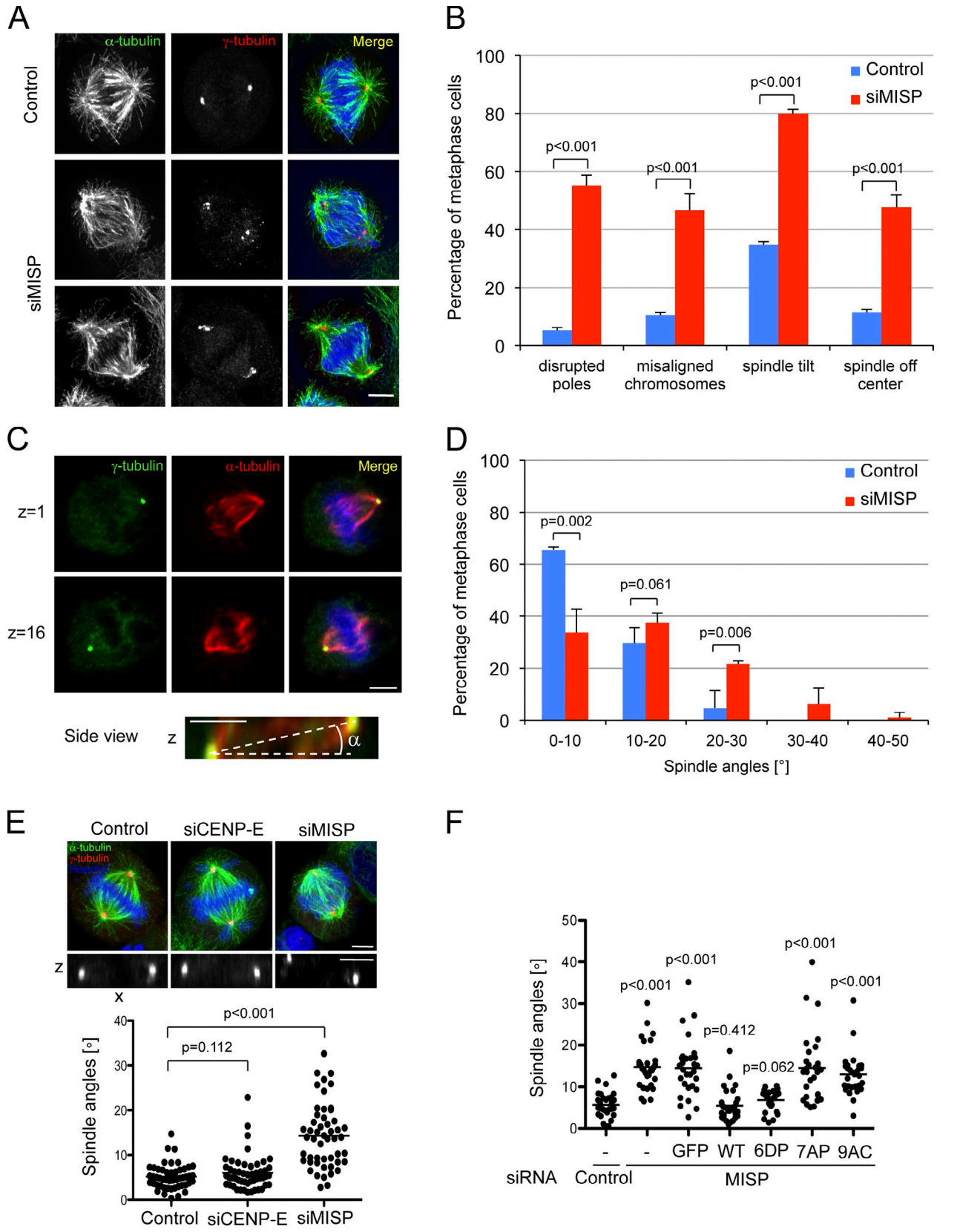

Figure 5. **Loss of MISP leads to spindle misorientation.** (A) HeLa cells treated with MISP or control siRNA for 48 h were stained for α-tubulin (green), γ-tubulin (red), and with Hoechst 33342 (blue). (B) Quantification of the described mitotic defects in control or MISP siRNA-treated cells. *n* = 50 cells each from three independent experiments. (C) Representative images of z-sections (0.4 µm per stack) with maximum spindle pole intensity and a side view of a 3D-reconstruction of the depicted cell with the spindle angle α. Cells were stained for α-tubulin (red), γ-tubulin (green), and Hoechst 33342 (blue). (D) Quantification of the percentage of metaphase cells with indicated spindle angles as described in C; *n* = 150 cells from three independent experiments. (E) HeLa cells treated with CENP-E, MISP, or control siRNA for 48 h were stained for α-tubulin (green), γ-tubulin (red), and with Hoechst 33342 (blue).

and S4 G; Chan et al., 2009; Dunsch et al., 2012), indicating a specific role of MISP in regulating this process. Moreover, spindle misorientation caused by MISP depletion can be rescued upon expression of MISP WT and the Plk1 phospho-mimetic MISP 6DP mutant but not the nonphosphorylatable MISP 7AP and 9AC mutants (Fig. 5 F). These results suggest that Plk1 phosphorylation positively regulates the function of MISP in spindle orientation.

Next, we set to analyze the consequence of the observed mitotic defects on cell survival. The detected severe malfunctions in mitotic progression led to a marked increase in the cleavage of the apoptotic marker PARP (Fig. S4 H), as well as a fivefold increase in AnnexinV-FITC–positive cells (Fig. S4 I). Therefore, the mitotic arrest caused by MISP ablation and the associated mitotic defects likely ultimately led to cell death.

MISP stabilizes astral microtubules

We then analyzed the mechanism of spindle misorientation induced by MISP depletion in more detail. Interactions of astral MTs with cortical structures are necessary for proper spindle orientation (Toyoshima and Nishida, 2007; Toyoshima et al., 2007). Quantification of the relative astral MTs signal intensity in fixed α-tubulin–stained cells demonstrated that MISP knockdown led to over 60% reduction in relative astral MT intensity compared with control cells (Fig. 6, A and B). The fluorescence intensity of the spindle MTs was comparable in both siRNA-treated cells (Fig. S5 A). Moreover, the spindle MTs in metaphase cells with aligned chromosomes were cold-stable after MISP depletion (Fig. S5 B) and also exhibited similar regrowth activity as control cells (Fig. S4 D), indicating that MISP depletion does not obviously alter the overall spindle microtubule stability and dynamics. To visualize the microtubule plus ends, we stained for the microtubule +TIP binding protein EB1 that plays a role in prompting microtubule assembly and stabilizing them at the growing ends (Hayashi et al., 2005). In ∼80% of the control metaphase cells, EB1 was found to track the plus-end tips of spindle MTs and astral MTs that interact with the cell cortex (Fig. 6 C, top inset); whereas in MISP-depleted cells, EB1 was present at the tips of spindle MTs, but only ∼34% of the cells showed EB1 signal near the cortex (Fig. 6 C, bottom inset). No difference in overall EB1 protein levels was observed (unpublished data). The reduced astral MTs were also observed in live-cell imaging tracked by EB3 (Videos 6 and 7). We propose that MISP knockdown disturbs the attachment of astral MTs to the cortex and thereby leading to their destabilization and shortening and thus spindle mispositioning. It was previously shown that astral MT interaction with the cell cortex participates in spindle orientation (Théry et al., 2005; Toyoshima and Nishida, 2007). Indeed, MISP can be detected in the vicinity of astral MTs at the cell cortex in fixed cells (Fig. 6 D). Given that MISP is an actin-binding protein (Fig. 3) and was not found to localize at the mitotic spindle (Fig. S3 A), the interaction between MISP and astral MTs is likely to be indirect. This was further confirmed by using an in vitro MT-binding assay. Unlike the MT-associated protein (MAPF), MISP was unable to efficiently copellet with taxol-polymerized MTs in vitro (Fig. S5 C). We speculate that MISP indirectly regulates astral MT stability probably by disassociating them from the cell cortex and microtubule stabilizers. The loss of astral MTs in MISP-depleted cells can be rescued after expression of MISP WT or 6DP mutant but not 7AP or 9AC mutants (Fig. 6 E), suggesting that Plk1 phosphorylation on MISP is required for stabilizing astral MTs and their cortical attachment.

MISP interacts with and regulates the cortical distribution of p150^{glued}

The cortically localized dynein–dynactin complex is known to play a crucial role in spindle orientation and positioning during embryonic and somatic cell divisions (Couwenbergs et al., 2007; Nguyen-Ngoc et al., 2007; Toyoshima et al., 2007; Kotak et al., 2012). To identify MISP-interacting proteins in regulation of spindle orientation, we performed a pull-down assay with GST-MISP using HeLa mitotic cell lysates followed by mass spectrometry analysis. In addition to actin, we also identified p150^{glued}, a subunit of the dynactin complex and a +TIP binding protein (Fig. S5 D). We first confirmed the interaction by endogenous p150^{glued} immunoprecipitation (Fig. 7 A). Next, we sought to investigate whether MISP would form a complex with microtubules and p150^{glued} in vivo. MTs from mitotic HeLa cells were polymerized or depolymerized by taxol or nocodazole treatment, respectively, and then pelleted by high-speed centrifugation. MISP appeared to cosediment with taxol-stabilized MTs together with p150^{glued} and actin, whereas MEK1/2 remained in the supernatant excluding cross-contamination with cytoplasmic proteins (Fig. 7 B). Previous findings also suggest that MISP associates with the mitotic spindle, as it was identified in mitotic spindle phosphoproteome (Nousiainen et al., 2006; Santamaria et al., 2011). However, depletion of either p150^{glued} or MISP did not reduce cosedimentation of the other with taxol-stabilized MTs from mitotic cells (Fig. S5 E), suggesting that cytoplasmic MISP might associate with spindle microtubules in vivo via other microtubule-binding protein(s). To examine the effects of MISP depletion on p150^{glued} localization, we treated HeLa cells with MISP or control siRNA and processed them for confocal immunofluorescence analysis after preextraction of the cytoplasm. p150^{glued} was found to localize at the spindle and astral microtubules, and cell cortex in control siRNA-treated cells (Fig. 7 C, top); whereas after MISP depletion, in addition to loss of the localization at astral MTs, ∼51% of the metaphase cells also showed accumulated and distributed

Top, representative images with z-projection; middle, the x-z projection of γ-tubulin signal; bottom, scatter plots of the spindle angles in control cells, CENP-E, or MISP-depleted cells (n = 50 cells from three independent experiments) with calculated mean value. (F) Scatter plots showing the spindle angles in control, MISP siRNA-treated cells with and without expression of GFP or siRNA-resistant versions of GFP-MISP WT/6DP/7AP/9AC (n = 30 cells from two independent experiments) with calculated mean value. Bars: (A, C, and E) 5 µm. Error bars in B and D represent SD. Student's t test was used to calculate p-values for comparison of control and experimental samples.

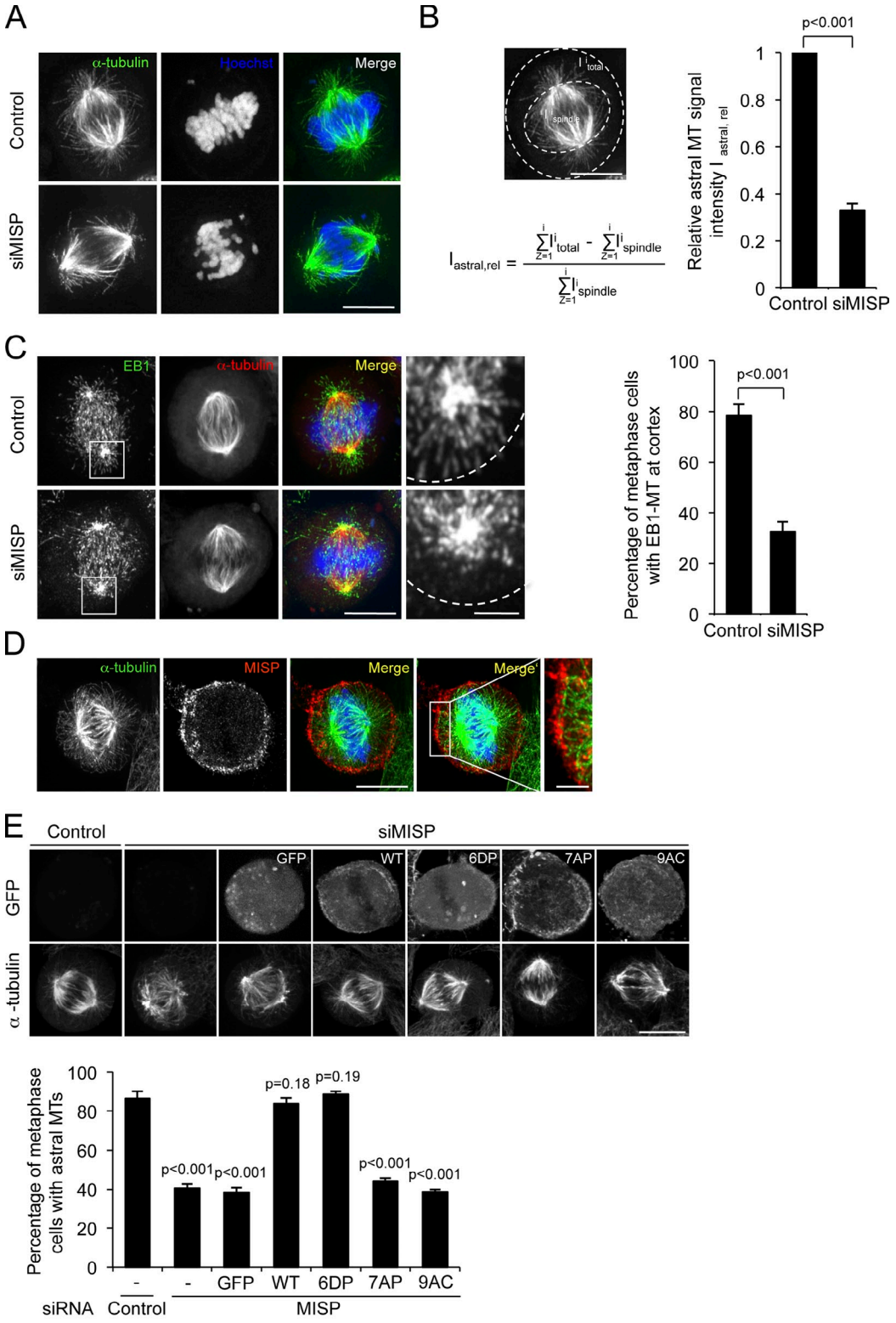

Figure 6. **MISP stabilizes astral MTs.** (A) MISP or control siRNA-treated HeLa cells were stained with α-tubulin (green) and Hoechst 33342 (blue). (B) Schematic overview and quantification of the observed metaphase spindles. The image is the control cell shown in A. The intensities of the spindle ($I_{spindle}$) and the total cell (I_{total}) were determined with ImageJ software. Relative astral MT intensity ($I_{astral,\ rel}$) was calculated by $[(I_{total} - I_{spindle})/I_{spindle}]$ and control value was set to 1. *n* = 20 cells each from three independent experiments. (C) RFP-tubulin HeLa stable cells were transfected with MISP or control siRNA and stained for EB1 (green) and Hoechst 33342 (blue). Enlargements of the insets show EB1 localization in the cortical region (dashed lines). Right panel shows quantification of the percentage of metaphase cells with EB1-MT at the cortex; *n* = 50 cells each from three independent experiments. (D) Co-staining of MISP (red), α-tubulin (green), and Hoechst 33342 (blue) in fixed HeLa cells. Inset shows higher magnification of the framed region. (E) HeLa cells transfected with control or MISP siRNA, or MISP siRNA under expression of GFP or siRNA-resistant versions of GFP-MISP WT/6DP/7AP/9AC were stained for α-tubulin. Top, representative images with z-projection; bottom, quantification of percentage of metaphase cells with astral MTs. Bars: (A, C–E) 10 µm; (C and D, insets) 2.5 µm. Error bars represent SD. Student's *t* test was used to calculate p-value for comparison of control and experimental samples.

cortical localization of p150^{glued} compared with ∼11% in the control siRNA-treated cells (Fig. 7, C and D). Next we investigated the impact of Plk1 phosphorylation on MISP in regulating p150^{glued} cortical recruitment. As shown in Fig. 7, E and F, the distributed p150^{glued} at the cortex could be partially rescued by expression of MISP WT and 6DP mutants but not 7AP or 9AC mutants, although there was no obvious difference in the binding of MISP WT and phospho-mutants to p150^{glued} (Fig. S5 F). Therefore, the regulation of the cortical distributed dynactin turnover by MISP is probably controlled through its effects on astral MTs. Taken together, these results indicate that MISP interacts with and regulates the distribution of dynactin at the cell cortex in a Plk1-dependent manner.

Discussion

Our data concur to identify the novel actin-binding protein MISP (C19orf21) as an important regulator of mitotic spindle orientation by stabilizing astral MT attachment to the cell cortex. As MISP is a so far uncharacterized protein, we analyzed the MISP sequence within different species including human, *Xenopus*, and *Drosophila* (Fig. S1 C). We identified uncharacterized sequence motifs, a conserved N-terminal region, a small repeated motif, and a conserved C-terminal region, which are also present in AKAP2 (AKAP-KL), a protein that is associated with the cortical actin cytoskeleton (Dong et al., 1998). Proteins of the AKAP family like pericentrin or AKAP450 are involved in microtubule nucleation and spindle pole integrity (Doxsey et al., 1994; Keryer et al., 2003). Moreover, moesin, the sole *Drosophila* member of the ERM (ezrin/radixin/moesin) family of proteins that includes the AKAP protein ezrin was shown to be required for cortical stability and spindle positioning (Carreno et al., 2008; Kunda et al., 2008). It is therefore tempting to speculate whether MISP is a new member of the AKAP family orchestrating actin cytoskeleton communication with astral MTs and regulating spindle positioning.

Once formed, the mitotic spindle must be properly positioned to establish the correct cell division plane. Insufficient attachment of the astral MT plus ends to the cell cortex causes spindle misorientation (Théry et al., 2005; Toyoshima and Nishida, 2007). However, the mechanisms controlling astral microtubule interactions at the cortex are poorly understood. Here we propose that MISP, a novel actin-binding protein, is involved in stabilizing astral MT attachment to the cortex during mitosis. Ablation of MISP function causes multiple mitotic defects, in particular spindle misorientation and a SAC-dependent delay in the metaphase-to-anaphase transition. Previous findings indicate that spindle misorientation could lead to a delayed anaphase onset in human cells, but most cells with misoriented spindles are eventually able to undergo anaphase (Delaval et al., 2011; Samora et al., 2011; Dunsch et al., 2012). How misoriented spindles prevent SAC satisfaction and cause mitotic delay still remains elusive. Although the majority of MISP-depleted cells properly aligned their chromosomes during early mitosis (Fig. 4 E), chromosome congression defects were observed afterward in both fixed cells and live-cell imaging caused by prolonged metaphase arrest (Fig. 5 B and Video 4). As shown in Fig. S3 F, the BubR1 signal was clearly detected in cells with misaligned chromosomes (middle panel), and also weakly observed in cells with aligned chromosomes (bottom panel) indicative of incomplete removal of SAC proteins. The slight BubR1 staining on the aligned chromosomes is probably due to insufficient kinetochore–microtubule attachments or lack of tension in the intra-kinetochore region between sister chromatids, thus delaying anaphase onset. It remains possible that MISP plays additional roles in spindle checkpoint regulation through other binding partners. Based on our live-cell imaging data, around half of MISP-depleted mitotic cells completed cell division during the monitored period, while the left mitotic cells with misoriented spindles ended with chromosome scattering or cell death, indicating roles of MISP in both spindle orientation and anaphase onset regulation. In this study, we characterized the function of MISP in the regulation of spindle orientation.

The most notable spindle orientation defect in the absence of MISP was a significant loss or shortening of astral MTs. This phenotype observed could be either caused by a failure of astral MT attachment to the cell cortex or by a defect in microtubule nucleation. However, a direct role of MISP in regulating the assembly of astral MT arrays is unlikely because we did not observe an obvious change in the levels of microtubule nucleating/elongation components such as γ-tubulin, Nedd1 (unpublished data), or EB1 (Fig. 6 C) at spindle poles during mitosis in response to MISP siRNA treatment. Furthermore, microtubule regrowth activity after MISP knockdown was similar as in the control cells after cold treatment (Fig. S4 D), ruling out microtubule nucleation problems. As MISP mainly localizes at the cell cortex and does not bind to microtubules directly, as shown in Fig. S5 C, we speculate that MISP regulates the stability of astral MTs probably through disturbing their binding to microtubule stabilizers at the tip of astral MTs. Thus, the identification of the linker protein(s) which regulate(s) the function of MISP on astral MTs will be of future interest and will help to understand the mitotic functions of MISP in detail.

Interestingly, we found that the role of MISP in both mitotic progression and spindle positioning is positively regulated through Plk1-dependent phosphorylation. A likely involvement of Plk1 in the regulation of spindle orientation has been demonstrated in two recent studies. Plk1 negatively regulates cortical dynein localization downstream of LGN-NuMA by controlling the interaction between dynein–dynactin and LGN–NuMA (Kiyomitsu and Cheeseman, 2012). In addition, Plk1-dependent phosphorylation of Dvl2, a Wnt signaling component that localizes to the spindle and spindle poles, regulates spindle orientation (Kikuchi et al., 2010). In this study, we show that Plk1 phosphorylation on MISP negatively regulates the cortical recruitment of p150^{glued}. Because the phospho-mimicking MISP 6DP mutant but not 7AP or 9AC was able to complement the distribution of p150^{glued} at the cortex (Fig. 7, E and F), Plk1 phosphorylation contributes to the function of MISP in this process, although it does not seem to be mediated by the MISP–p150^{glued} interaction (Fig. S5 F). We speculate that the mechanism on how MISP regulates cortical localized p150^{glued} could be a consequence of its impact on astral MTs, which facilitate the microtubule minus end (spindle pole)–directed transport of the cortical localized

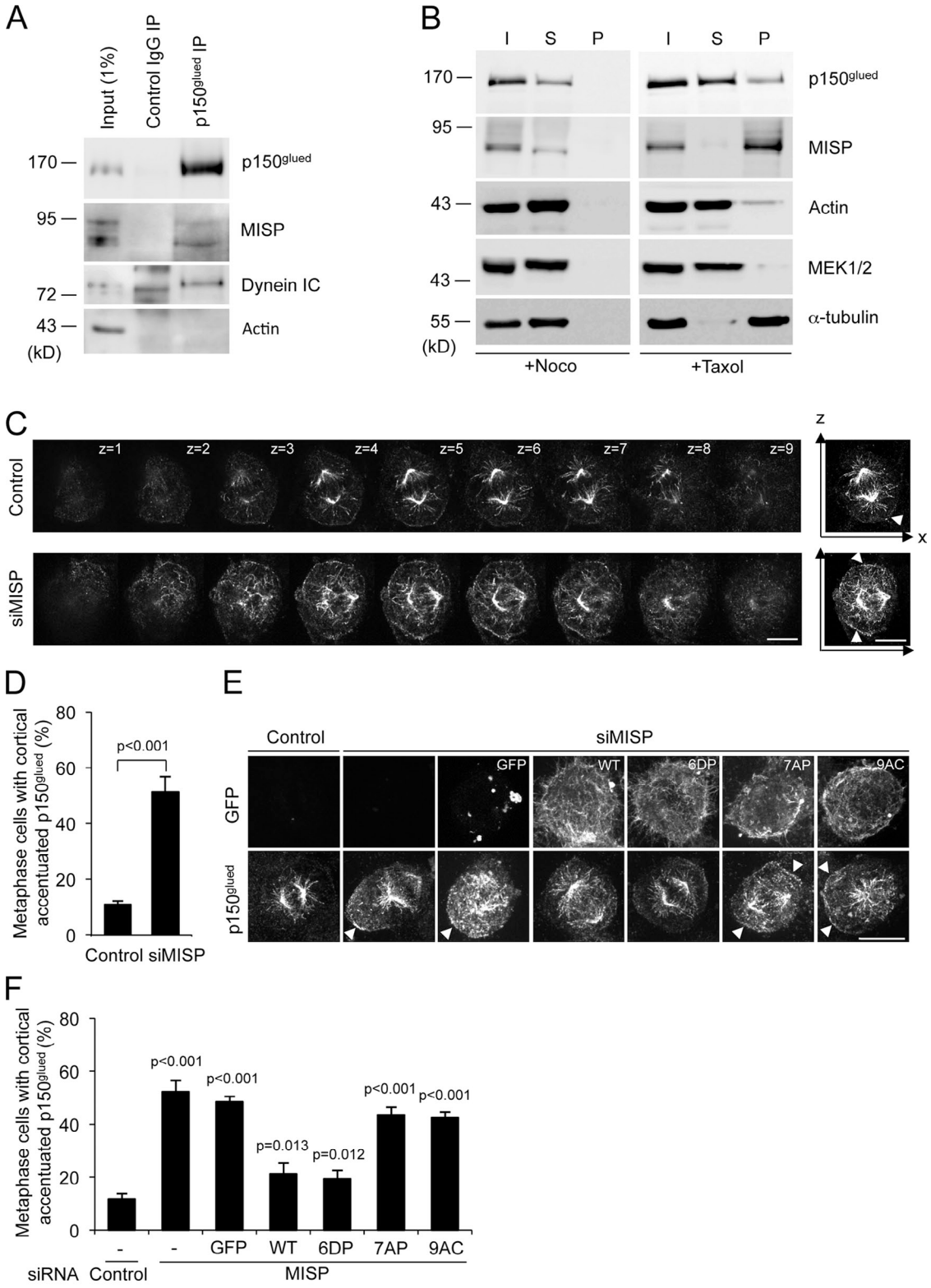

Figure 7. **MISP associates with p150glued and regulates its distribution at the cortex.** (A) p150glued was immunoprecipitated from nocodazole-blocked HeLa cells and analyzed by Western blot with indicated antibodies. Asterisk, unspecific recognized band in the control mouse IgG immunoprecipitate. (B) MTs were pelleted by high-speed centrifugation after nocodazole or taxol incubation. Input (I), supernatant (S), and the pellet (P) were analyzed by Western blot with indicated antibodies. (C) Z-stack images (0.4 µm per stack) of p150glued in metaphase HeLa cells depleted with MISP or control siRNA after cytoplasmic extraction. Right panel shows images with x-z projection. Arrowheads show the cortical localized p150glued. (D) Quantification of the percentage of metaphase cells with cortical accentuated and distributed p150glued; *n* = 50 cells each from three independent experiments. (E) HeLa cells transfected with control or MISP siRNA, or MISP siRNA under expression of GFP or siRNA-resistant versions of GFP-MISP WT/6DP/7AP/9AC were stained for p150glued. Representative images with z-projection are shown. Arrowheads indicate the cortical localized p150glued. (F) Quantification of the percentage of metaphase cells with cortical accentuated and distributed p150glued. *n* = 50 cells each from three independent experiments. Bars: (C and E) 10 µm. Error bars in D and F represent SD. Student's *t* test was used to calculate p-value for comparison of control and experimental samples.

dynein–dynactin complex. Moreover, our findings also suggest that constant turnover of dynein–dynactin complex at the cortical region is required for proper spindle positioning. Collectively, we provide evidence that Plk1 phosphorylates MISP localized at the cortex to control interactions of actin filaments with astral MTs, thereby regulating spindle orientation and anaphase onset.

Materials and methods

Cell culture, cell synchronization, and transfection

HeLa cells were grown in DME (Sigma-Aldrich) medium containing 1 g/l glucose, 10% fetal calf serum (PAA), and 2 mM glutamine (Invitrogen). For HeLa Kyoto RFP-α-tubulin stable cells, the same medium was used supplemented with 0.5 µg/ml puromycin; 500 µg/ml G418 was supplemented for culturing GFP-H2B HeLa Kyoto stable cell line; 500 µg/ml G418 and 0.5 µg/ml puromycin for GFP-α-tubulin/RFP-H2B cells.

To arrest cells in mitosis, they were treated with 100 ng/ml nocodazole for 16 h. Cells were released after mitotic shake-off into 10 µM MG132 containing medium for 3 h to obtain metaphase-arrested cells or followed by release for 1.5 h in normal DME medium to obtain cells in late mitotic stages. For the double thymidine block, cells were treated with 4 mM thymidine for 20 h, then released for 14 h and again blocked for 16 h.

HeLa cells were transfected with Ca^{2+}-phosphate according to standard protocols. For siRNA transfections and plasmid DNA transfections, HeLa cells were transfected with Lipofectamine 2000 (Invitrogen) according to the manufacturer's instructions.

Antibodies

A rabbit polyclonal antibody was raised against the full-length GST-MISP protein that was expressed as a GST fusion in *Escherichia coli* (Innovagen). The antibody was purified using the corresponding protein immobilized on CNBr-activated Sepharose. Other antibodies used in this study: mouse anti-Plk1 (F8 and 36–298), mouse anti-Cdk1 (p34), and rabbit anti-GST (Z5), purchased from Santa Cruz Biotechnology, Inc.; rabbit anti-cyclin B1 was generated against full-length human Cyclin B1 purified from *E. coli* as described previously (Hoffmann et al., 1993); mouse anti-Flag M2, mouse anti-BubR1 (8G1), human anti–AnnexinV-FITC conjugate, mouse anti–γ-tubulin (GTU-88), and mouse anti–α-tubulin were obtained from Sigma-Aldrich; mouse anti-actin (JLA20) was from EMD Millipore; mouse anti-$p150^{glued}$, mouse anti-PARP, mouse anti-actin (C4), and mouse anti-EB1 were from BD; rabbit anti-Mad2 (PRB452C) was obtained from Covance; rabbit anti-GFP antibody was obtained from Novus Biologicals; rabbit anti-phosphohistone H3 Ser10 (6G3) and rabbit anti-MEK1/2 were from Cell Signaling Technology; rabbit anti-pericentrin from A. Merdes (CNRS, Toulouse, France); rabbit anti-Cep135 from R. Kuriyama (University of Minnesota, Minneapolis, MN). Mouse anti-CENP-E (1H12) was from Abcam; mouse anti-dynein intermediate chain (IC) was purchased from Sigma-Aldrich (clone 70.1). Peroxidase-conjugated donkey anti–rabbit and goat anti–mouse antibodies were purchased from Jackson ImmunoResearch Laboratories, Inc.; Alexa Fluor 488 and 594 anti–mouse and Alexa Fluor 488 and 594 anti–rabbit were purchased from Invitrogen. Atto 488 Phalloidin was purchased from Sigma-Aldrich.

Molecular cloning

MISP (DKFZp686H18209) was received from S. Wiemann (DKFZ, Heidelberg, Germany), PCR amplified and cloned into the XhoI–BamHI sites of the pEGFP-C1 (Takara Bio Inc.), the BamHI–XhoI sites of pGEX-4T3 (GE Healthcare), and of pCMV-3Tag-1 (Agilent Technologies). All MISP fragments were PCR amplified and cloned into the BamHI–XhoI sites of pCMV-3Tag-1. pRcCMV-Plk1 was received from S. Lev (Weizmann Institute, Rehovot, Israel), PCR amplified and cloned into the EcoRI–XhoI sites of pGEX-4T1 and the EcoRI–XhoI sites of pCMV-3Tag-1. The Plk1 PBD was also PCR amplified and cloned into the EcoRI–XhoI sites of pGEX-4T1. pEGFP-EB3 (pEGFP-N1; Takara Bio Inc.) was a kind gift from L. Wordeman (University of Washington, Seattle, WA; Stepanova et al., 2003).

Recombinant protein expression

All recombinant proteins were expressed in *E. coli* BL21-Rosetta. Bacteria were grown in LB medium at 30°C and protein expression was induced with 1 mM isopropylthio-β-D-galactoside for 16 h at 18°C. MISP WT/6DP/7AP/9AC and the Plk1 PBD carrying an N-terminal GST tag were natively purified by single-step affinity chromatography using GST-Sepharose according to the manufacturer's instructions.

Interaction experiments and kinase assays

For coimmunoprecipitations, 1–8 mg of cell lysate were incubated with 1–7 µg of specific antibodies in NP-40 buffer (40 mM Tris, pH 7.5, 150 mM NaCl, 0.5% NP-40, 5 mM EDTA, 10 mM β-glycerophosphate, and 5 mM NaF) or RIPA buffer (50 mM Tris, pH 7.5, 150 mM NaCl, 1% NP-40, and 0.5% deoxycholate) for 4 h at 4°C and collected by addition of 10 µl protein G–Sepharose (GE Healthcare). After extensive washing, the beads were denatured at 95°C in 2× SDS buffer and analyzed by SDS-PAGE and Western blot. Far Western ligand blots were performed in TBST (50 mM Tris-HCl, pH 7.4, 137 mM NaCl, 0.1% Tween 20, and 4% [wt/vol] skim milk powder) as described previously (Neef et al., 2003). Flag-vector or Flag-MISP WT/phospho-mutant transfected HeLa cell lysates were separated on SDS-PAGE followed by blotting on a nitrocellulose membrane. Bacterially purified GST-PBD or GST-FAM was incubated with the membrane, respectively. Bound proteins were detected using rabbit antibodies to GST and mouse anti-Flag M2 antibodies, respectively.

For in vitro pull-down experiments, GST-Plk1 or GST-MISP was immobilized on GST-Sepharose beads and incubated for 3 h at 4°C with mitotic HeLa lysates in pull-down buffer (50 mM Tris, pH 7.5, 150 mM NaCl, 10 mM β-glycerophosphate, 5 mM NaF, 5 mM $MgCl_2$, and 5% glycerol). Beads were washed three times with pull-down buffer and eluted once with pull-down buffer + 50 mM NaCl and once with pull-down buffer + 850 mM NaCl. After TCA precipitation, bound proteins were analyzed by SDS-PAGE and Western blot or silver staining followed by subsequent mass spectrometry.

To assay Plk1 and Cdk1 kinase activities, His-Plk1 (EMD Millipore) or GST-Cyclin B/His-Cdk1 (EMD Millipore) was incubated with bacterially purified recombinant GST-MISP wt/7AP/9AC as substrates for 30 min at 30°C in kinase assay buffer (50 mM Tris, pH 7.5, 5 mM $MgCl_2$, and 1 mM DTT) supplemented with 50 µM ATP and 2.5 µCi of γ-[^{32}P]ATP (PerkinElmer), and analyzed by autoradiography after SDS-PAGE. Kinase activities were inhibited by BI2536 (Boehringer Ingelheim) and roscovitine (Sigma-Aldrich) for Plk1 and Cdk1, respectively.

siRNAs

siRNAs used in this study were directed against the following sequences: MISP Ol1, 5′-ACUCGGUGUCUGAGUCUCCCUUCUU-3′; MISP Ol2, 5′-GUGUCCAAGUUGUGGAUGAtt-3′; Plk1, 5′-GGGCGGCUUUGCCAAGUGCtt-3′; Mad2, 5′-UGAACAAGAAACUUCCAACAGUGGC-3′; firefly luciferase GL2 (control), 5′-CGUACGCGGAAUACUUUCGAtt-3′; CENP-E, 5′-AACACGGAUGCUGGUGACCUC-3′; $p150^{glued}$, 5′-GAUCGAGAGACAGUUAUUAtt-3′. MISP Ol1 was purchased from Invitrogen and Mad2 siRNA was a gift from O. Gruss (ZMBH, Heidelberg, Germany). All other siRNAs were purchased from Applied Biosystems.

Immunofluorescence microscopy and live-cell imaging

Cells grown on coverslips were either fixed with ice-cold methanol for 10 min at −20°C, or with 3.7% formaldehyde at RT for 10 min or with 4% paraformaldehyde at RT for 10 min. For cytoplasmic extraction, cells were pretreated with PHEM buffer (60 mM Pipes, pH 6.9, 25 mM Hepes, 10 mM EGTA, 2 mM $MgCl_2$, 0.5% Triton X-100, and 10 µM taxol) for 1 min at RT. They were washed with PBS and blocked with 3% BSA/PBS for 30 min. Cells were then incubated with primary antibodies for 2 h and with Alexa Fluor 488– or Alexa Fluor 594–conjugated secondary antibodies for 1 h at RT. DNA was stained with Hoechst 33342 (Molecular Probes). Cells were washed three times with PBS in between antibody incubations at RT. Coverslips were mounted in Mowiol 4-88 mounting medium. Images were taken with a spinning disk confocal system (UltraView ERS-6; PerkinElmer) and 100× NA 1.40 oil immersion objective on an inverted microscope (Ti; Nikon) connected to an electron multiplying charge-coupled device camera (Hamamatsu Photonics) in the Nikon Imaging Center (University of Heidelberg, Heidelberg, Germany). Lasers of 405-, 488-, 561-, and 640-nm wavelength were used for fluorochrome excitation. Z-stacks were taken at an interval of 0.2 or 0.4 µm by Volocity software (PerkinElmer) and maximum intensity projection was performed using ImageJ software (National Institutes of Health). Relative astral MT intensities were calculated within the equatorial stack defined by spindle pole maximum intensity using ImageJ software to create 8-bit RGB TIFF files. Images were then processed with Photoshop CS3 (Adobe Systems) to produce the figures.

For live-cell imaging experiments, HeLa Kyoto GFP-α-tubulin/RFP-H2B cells were grown in a Lab-Tek II chambered coverglass (8 chamber) for 24 h after siRNA transfection and were monitored afterward by a TIRF 40× NA 1.30 oil immersion objective (Nikon) on an inverted microscope (Ti; Nikon) connected to an electron multiplying charge-coupled device camera (iXon DU-897; Andor Technology) at 5% CO_2, 37°C, 90% humidity.

Lasers of 488- and 561-nm wavelength were used for fluorochrome excitation. Multi-point images were taken with 9 z-stacks spaced 2 µm apart every 6 min for 8 h by NIS-Elements software (Nikon) and were deconvolved using Huygens deconvolution software (Scientific Volume Imaging). HeLa Kyoto GFP-H2B cells were grown in a Lab-Tek II chambered coverglass (4 chamber) for 28 h after siRNA transfection and were monitored afterward by a spinning disk confocal system (UltraView ERS-VoX; PerkinElmer) with an inverted microscope (Ti; Nikon) with a 40× NA 1.30 oil immersion objective at 5% CO_2, 37°C, 90% humidity. Multi-point images were taken with 9 z-stacks spaced 2 µm apart every 3 min for 8–12 h by Volocity software. Phase-contrast images were taken with one z-stack in the middle position. For the EB3 tracking experiment, GFP-EB3 was transiently transfected into HeLa cells followed by MISP siRNA treatment for 48 h. 7 planes spaced apart by 0.5 µm were captured with the maximum rate of 1 min (60× NA 1.30 oil immersion objective) by Volocity software. Maximum intensity projection of the fluorescent channels was performed by ImageJ software to create 8-bit RGB TIFF files and movies.

Spindle positioning assay

HeLa cells plated on fibronectin-coated coverslips were transfected with control, CENP-E, or MISP siRNA, or MISP siRNA under expression of siRNA-resistant versions of GFP-MISP WT or phospho-mutants for 48 h. Cells showing a congressed metaphase plate were analyzed for spindle orientation by confocal imaging with z-sections (0.4 µm per stack). Spindle angle was calculated with the sinus-function by measuring the distance in x- and z-direction between the maximum intensities of the spindle poles using Imaris (Bitplane, Inc.) or ImageJ software.

Actin cosedimentation assay

The actin cosedimentation assays were done by following the instructions of the Non-Muscle Actin Binding Protein Spin-Down Biochem kit (catalog no. BK013) from Cytoskeleton. Samples were centrifuged at 150,000 *g* for 1.5 h using a TLA100.3 rotor (Beckman Coulter) at 24°C. The pellet was resuspended in 1× Laemmli buffer and analyzed together with the supernatant by SDS-PAGE.

In vitro MT-binding assay

The in vitro MT cosedimentation assays were performed following the instructions of the Microtubule Binding Protein Spin-Down Assay Biochem kit (catalog no. BK029) from Cytoskeleton. Samples were centrifuged at 100,000 *g* for 40 min using the TLA100.3 rotor (Beckman Coulter) at 22°C. The pellet was resuspended in 1× Laemmli buffer and was analyzed along with the supernatant by SDS-PAGE. MAPF (MT-associated protein fraction containing 60% MAP2 and 40% tau proteins) was included in the kit as a positive control.

MT cosedimentation assay

Mitotic HeLa cells were resuspended in PEM buffer (80 mM Pipes, pH 6.9, 1 mM EGTA, 1 mM $MgCl_2$, and 0.5% NP-40), incubated at 4°C for 15 min, and sonicated four times for 15 s each. Cleared lysates were incubated with 10 µM taxol or nocodazole (negative control), 1 mM GTP, 1 mM AMP-PNP, and 8% 2-methyl-2,4-pentanediol (Sigma-Aldrich) for 30 min at 30°C and layered over a 25% glycerol cushion in PEM buffer. After centrifugation at 48,000 rpm in a TLS55 rotor (Beckman Coulter), the resulting pellets were resuspended in 0.2 volumes PEM buffer + 10 µM taxol or nocodazole and were recentrifuged as described above. The final MT pellets were resuspended in 1× SDS buffer and analyzed by SDS-PAGE and Western blot together with supernatant.

MT regrowth assay

MTs were depolymerized by cold treatment for 30 min at 4°C. Repolymerization of MTs was then achieved by addition of prewarmed medium and a temperature shift back to 37°C for 0, 1, and 5 min.

FACS analysis

For cell cycle analysis, cells were fixed with 70% ice-cold ethanol and DNA content was analyzed by propidium iodide staining (50 µg/ml) in FACS buffer (38 mM NaCitrate and 1 µg/ml RNase A) on a FACSort cytometer (BD). For annexin staining, AnnexinV-FITC (Sigma-Aldrich) was used as described in the manufacturer's procedure. In brief, cells were resuspended in binding buffer (10 mM Hepes, pH 7.5, 140 mM NaCl, and 2.5 mM $CaCl_2$) and incubated with 25 µg/ml AnnexinV-FITC and 50 µg/ml propidium iodide for 10 min at RT before analysis on the FACSort.

Computational sequence analysis and comparison of MISP

The initial sequence similarity searches were performed with BLAST (Altschul et al., 1997) against the nonredundant protein sequence database Uniref50 (Wu et al., 2006). Multiple sequence alignments of homologous protein sequences were generated with the program T-Coffee (Notredame et al., 2000) using default parameters that were slightly refined manually. Profiles of the alignment as global hidden Markov models (HMMs) were generated using HMMer (Eddy, 1995). Iterative similarity searches (E-value inclusion threshold < 0.005), using HMMer (Eddy, 1995), with the repeated region identified in the three vertebrate paralogues (MISP, AKAP2, and LOC113230, UniProt: Q8IVT2_HUMAN, Q9Y2D5_HUMAN, Q96FF7_HUMAN, respectively) as query identified remote homologues including: urochordates (*Ciona intestinalis* and *Oikopleura dioica*), hemichordates (*Saccoglossus kowalevskii*), equinoderms (*Strongylocentrotus purpuratus*), cnidarians (*Nematostella vectensis*), mollusks (*Lottia gigantea* and *Crassostrea gigas*), annelids (*Capitella teleta* and *Helobdella robusta*), and arthropods (*Daphnia pulex*, *Anopheles gambiae*, and, *Ixodes scapularis*, among others), including the *Drosophila melanogaster* CG2556 protein, UniProt: Q9VYM2_DROME. Sequences were obtained from UniProt, JGI (Joint Genome Institute), NCBI-GenBank, and NCBI-dbEST but were supplemented by manually assembled ESTs and FGENESH+ predicted gene models (Solovyev et al., 2006).

Online supplemental material

Fig. S1 shows the identification and characterization of MISP, and its binding activity to Plk1. Fig. S2 shows the identification of the mitotic phosphorylation sites on MISP and the localization of Flag-MISP WT and phospho-mutants in HeLa cells. Fig. S3 shows that MISP is required for mitotic progression. Fig. S4 shows that MISP knockdown leads to mitotic defects and apoptosis. Fig. S5 shows that MISP does not directly bind to MTs and associates with $p150^{glued}$ in a phosphorylation-independent manner. Videos 1 and 2 show mitotic progression in MISP siRNA-treated GFP-α-tubulin/RFP-H2B HeLa cells. Video 3 shows mitotic progression in control siRNA-treated GFP-α-tubulin/RFP-H2B HeLa cells. Video 4 shows mitotic progression in MISP siRNA-treated GFP-H2B HeLa cells. Video 5 shows mitotic progression in control siRNA-treated GFP-H2B HeLa cells. Video 6 shows spindle microtubule dynamics tracked by GFP-EB3 in MISP siRNA-treated HeLa cells. Video 7 shows spindle microtubule dynamics tracked by GFP-EB3 in control siRNA-treated HeLa cells. Online supplemental material is available at http://www.jcb.org/cgi/content/full/jcb.201207050/DC1. Additional data are available in the JCB DataViewer at http://dx.doi.org/10.1083/jcb.201207050.dv.

We thank O. Gruss, S. Lev, A. Merdes, L. Wordeman, R. Kuriyama, and S. Wiemann for reagents. We acknowledge Ulrike Engel, Christian Ackermann, and Peter Bankhead from the Nikon Imaging Center at the University of Heidelberg for equipment and assistance in implementation of experiments.

This work was supported by the DKFZ-MOST program and the Deutsche Krebshilfe (110243) both to I. Hoffmann, the von Humboldt Foundation (to M. Zhu) as well as the EMBO (ALTF 366-2009 to S. Kotak), and the Swiss National Science Foundation (3100A0-122500/1 to P. Gönczy).

Submitted: 6 July 2012
Accepted: 13 February 2013

References

Ahringer, J. 2003. Control of cell polarity and mitotic spindle positioning in animal cells. *Curr. Opin. Cell Biol.* 15:73–81. http://dx.doi.org/10.1016/S0955-0674(02)00018-2

Altschul, S.F., T.L. Madden, A.A. Schäffer, J. Zhang, Z. Zhang, W. Miller, and D.J. Lipman. 1997. Gapped BLAST and PSI-BLAST: a new generation of protein database search programs. *Nucleic Acids Res.* 25:3389–3402. http://dx.doi.org/10.1093/nar/25.17.3389

Bowman, S.K., R.A. Neumüller, M. Novatchkova, Q. Du, and J.A. Knoblich. 2006. The *Drosophila* NuMA homolog Mud regulates spindle orientation in asymmetric cell division. *Dev. Cell.* 10:731–742. http://dx.doi.org/10.1016/j.devcel.2006.05.005

Carreno, S., I. Kouranti, E.S. Glusman, M.T. Fuller, A. Echard, and F. Payre. 2008. Moesin and its activating kinase Slik are required for cortical stability and microtubule organization in mitotic cells. *J. Cell Biol.* 180:739–746. http://dx.doi.org/10.1083/jcb.200709161

Chan, Y.W., L.L. Fava, A. Uldschmid, M.H. Schmitz, D.W. Gerlich, E.A. Nigg, and A. Santamaria. 2009. Mitotic control of kinetochore-associated

dynein and spindle orientation by human Spindly. *J. Cell Biol.* 185:859–874. http://dx.doi.org/10.1083/jcb.200812167

Couwenbergs, C., J.C. Labbé, M. Goulding, T. Marty, B. Bowerman, and M. Gotta. 2007. Heterotrimeric G protein signaling functions with dynein to promote spindle positioning in *C. elegans*. *J. Cell Biol.* 179:15–22. http://dx.doi.org/10.1083/jcb.200707085

Daum, J.R., T.A. Potapova, S. Sivakumar, J.J. Daniel, J.N. Flynn, S. Rankin, and G.J. Gorbsky. 2011. Cohesion fatigue induces chromatid separation in cells delayed at metaphase. *Curr. Biol.* 21:1018–1024. http://dx.doi.org/10.1016/j.cub.2011.05.032

Delaval, B., A. Bright, N.D. Lawson, and S. Doxsey. 2011. The cilia protein IFT88 is required for spindle orientation in mitosis. *Nat. Cell Biol.* 13:461–468. http://dx.doi.org/10.1038/ncb2202

Dong, F., M. Feldmesser, A. Casadevall, and C.S. Rubin. 1998. Molecular characterization of a cDNA that encodes six isoforms of a novel murine A kinase anchor protein. *J. Biol. Chem.* 273:6533–6541. http://dx.doi.org/10.1074/jbc.273.11.6533

Doxsey, S.J., P. Stein, L. Evans, P.D. Calarco, and M. Kirschner. 1994. Pericentrin, a highly conserved centrosome protein involved in microtubule organization. *Cell*. 76:639–650. http://dx.doi.org/10.1016/0092-8674(94)90504-5

Du, Q., and I.G. Macara. 2004. Mammalian Pins is a conformational switch that links NuMA to heterotrimeric G proteins. *Cell*. 119:503–516. http://dx.doi.org/10.1016/j.cell.2004.10.028

Dunsch, A.K., D. Hammond, J. Lloyd, L. Schermelleh, U. Gruneberg, and F.A. Barr. 2012. Dynein light chain 1 and a spindle-associated adaptor promote dynein asymmetry and spindle orientation. *J. Cell Biol.* 198:1039–1054. http://dx.doi.org/10.1083/jcb.201202112

Eddy, S.R. 1995. Multiple alignment using hidden Markov models. *Proc. Int. Conf. Intell. Syst. Mol. Biol.* 3:114–120.

Elia, A.E., L.C. Cantley, and M.B. Yaffe. 2003a. Proteomic screen finds pSer/pThr-binding domain localizing Plk1 to mitotic substrates. *Science*. 299:1228–1231. http://dx.doi.org/10.1126/science.1079079

Elia, A.E., P. Rellos, L.F. Haire, J.W. Chao, F.J. Ivins, K. Hoepker, D. Mohammad, L.C. Cantley, S.J. Smerdon, and M.B. Yaffe. 2003b. The molecular basis for phosphodependent substrate targeting and regulation of Plks by the Polo-box domain. *Cell*. 115:83–95. http://dx.doi.org/10.1016/S0092-8674(03)00725-6

Fink, J., N. Carpi, T. Betz, A. Bétard, M. Chebah, A. Azioune, M. Bornens, C. Sykes, L. Fetler, D. Cuvelier, and M. Piel. 2011. External forces control mitotic spindle positioning. *Nat. Cell Biol.* 13:771–778. http://dx.doi.org/10.1038/ncb2269

Gönczy, P. 2008. Mechanisms of asymmetric cell division: flies and worms pave the way. *Nat. Rev. Mol. Cell Biol.* 9:355–366. http://dx.doi.org/10.1038/nrm2388

Grill, S.W., J. Howard, E. Schäffer, E.H. Stelzer, and A.A. Hyman. 2003. The distribution of active force generators controls mitotic spindle position. *Science*. 301:518–521. http://dx.doi.org/10.1126/science.1086560

Hayashi, I., A. Wilde, T.K. Mal, and M. Ikura. 2005. Structural basis for the activation of microtubule assembly by the EB1 and p150Glued complex. *Mol. Cell*. 19:449–460. http://dx.doi.org/10.1016/j.molcel.2005.06.034

Hoffmann, I., P.R. Clarke, M.J. Marcote, E. Karsenti, and G. Draetta. 1993. Phosphorylation and activation of human cdc25-C by cdc2—cyclin B and its involvement in the self-amplification of MPF at mitosis. *EMBO J.* 12:53–63.

Johmura, Y., N.K. Soung, J.E. Park, L.R. Yu, M. Zhou, J.K. Bang, B.Y. Kim, T.D. Veenstra, R.L. Erikson, and K.S. Lee. 2011. Regulation of microtubule-based microtubule nucleation by mammalian polo-like kinase 1. *Proc. Natl. Acad. Sci. USA*. 108:11446–11451. http://dx.doi.org/10.1073/pnas.1106223108

Keryer, G., B. Di Fiore, C. Celati, K.F. Lechtreck, M. Mogensen, A. Delouvee, P. Lavia, M. Bornens, and A.M. Tassin. 2003. Part of Ran is associated with AKAP450 at the centrosome: involvement in microtubule-organizing activity. *Mol. Biol. Cell*. 14:4260–4271. http://dx.doi.org/10.1091/mbc.E02-11-0773

Kikuchi, K., Y. Niikura, K. Kitagawa, and A. Kikuchi. 2010. Dishevelled, a Wnt signalling component, is involved in mitotic progression in cooperation with Plk1. *EMBO J.* 29:3470–3483. http://dx.doi.org/10.1038/emboj.2010.221

Kiyomitsu, T., and I.M. Cheeseman. 2012. Chromosome- and spindle-pole-derived signals generate an intrinsic code for spindle position and orientation. *Nat. Cell Biol.* 14:311–317. http://dx.doi.org/10.1038/ncb2440

Kotak, S., C. Busso, and P. Gönczy. 2012. Cortical dynein is critical for proper spindle positioning in human cells. *J. Cell Biol.* 199:97–110. http://dx.doi.org/10.1083/jcb.201203166

Kunda, P., A.E. Pelling, T. Liu, and B. Baum. 2008. Moesin controls cortical rigidity, cell rounding, and spindle morphogenesis during mitosis. *Curr. Biol.* 18:91–101. http://dx.doi.org/10.1016/j.cub.2007.12.051

Mao, Y., A. Abrieu, and D.W. Cleveland. 2003. Activating and silencing the mitotic checkpoint through CENP-E-dependent activation/inactivation of BubR1. *Cell*. 114:87–98. http://dx.doi.org/10.1016/S0092-8674(03)00475-6

Mimori-Kiyosue, Y., and S. Tsukita. 2003. "Search-and-capture" of microtubules through plus-end-binding proteins (+TIPs). *J. Biochem.* 134:321–326. http://dx.doi.org/10.1093/jb/mvg148

Musacchio, A., and E.D. Salmon. 2007. The spindle-assembly checkpoint in space and time. *Nat. Rev. Mol. Cell Biol.* 8:379–393. http://dx.doi.org/10.1038/nrm2163

Neef, R., C. Preisinger, J. Sutcliffe, R. Kopajtich, E.A. Nigg, T.U. Mayer, and F.A. Barr. 2003. Phosphorylation of mitotic kinesin-like protein 2 by polo-like kinase 1 is required for cytokinesis. *J. Cell Biol.* 162:863–875. http://dx.doi.org/10.1083/jcb.200306009

Nguyen-Ngoc, T., K. Afshar, and P. Gönczy. 2007. Coupling of cortical dynein and G alpha proteins mediates spindle positioning in *Caenorhabditis elegans*. *Nat. Cell Biol.* 9:1294–1302. http://dx.doi.org/10.1038/ncb1649

Notredame, C., D.G. Higgins, and J. Heringa. 2000. T-Coffee: A novel method for fast and accurate multiple sequence alignment. *J. Mol. Biol.* 302:205–217. http://dx.doi.org/10.1006/jmbi.2000.4042

Nousiainen, M., H.H. Silljé, G. Sauer, E.A. Nigg, and R. Körner. 2006. Phosphoproteome analysis of the human mitotic spindle. *Proc. Natl. Acad. Sci. USA*. 103:5391–5396. http://dx.doi.org/10.1073/pnas.0507066103

O'Connell, C.B., and Y.L. Wang. 2000. Mammalian spindle orientation and position respond to changes in cell shape in a dynein-dependent fashion. *Mol. Biol. Cell*. 11:1765–1774.

Petronczki, M., P. Lénárt, and J.M. Peters. 2008. Polo on the rise-from mitotic entry to cytokinesis with Plk1. *Dev. Cell*. 14:646–659. http://dx.doi.org/10.1016/j.devcel.2008.04.014

Rogers, S.L., G.C. Rogers, D.J. Sharp, and R.D. Vale. 2002. *Drosophila* EB1 is important for proper assembly, dynamics, and positioning of the mitotic spindle. *J. Cell Biol.* 158:873–884. http://dx.doi.org/10.1083/jcb.200202032

Samora, C.P., B. Mogessie, L. Conway, J.L. Ross, A. Straube, and A.D. McAinsh. 2011. MAP4 and CLASP1 operate as a safety mechanism to maintain a stable spindle position in mitosis. *Nat. Cell Biol.* 13:1040–1050. http://dx.doi.org/10.1038/ncb2297

Santamaria, A., B. Wang, S. Elowe, R. Malik, F. Zhang, M. Bauer, A. Schmidt, H.H. Sillje, R. Korner, and E.A. Nigg. 2011. The Plk1-dependent phosphoproteome of the early mitotic spindle. *Mol. Cell. Proteomics.* 10:M110 004457.

Schuyler, S.C., and D. Pellman. 2001. Microtubule "plus-end-tracking proteins": The end is just the beginning. *Cell*. 105:421–424. http://dx.doi.org/10.1016/S0092-8674(01)00364-6

Siller, K.H., C. Cabernard, and C.Q. Doe. 2006. The NuMA-related Mud protein binds Pins and regulates spindle orientation in *Drosophila* neuroblasts. *Nat. Cell Biol.* 8:594–600. http://dx.doi.org/10.1038/ncb1412

Solovyev, V., P. Kosarev, I. Seledsov, and D. Vorobyev. 2006. Automatic annotation of eukaryotic genes, pseudogenes and promoters. *Genome Biol*. 7:S10.1–12.

Stepanova, T., J. Slemmer, C.C. Hoogenraad, G. Lansbergen, B. Dortland, C.I. De Zeeuw, F. Grosveld, G. van Cappellen, A. Akhmanova, and N. Galjart. 2003. Visualization of microtubule growth in cultured neurons via the use of EB3-GFP (end-binding protein 3-green fluorescent protein). *J. Neurosci.* 23:2655–2664.

Stevens, D., R. Gassmann, K. Oegema, and A. Desai. 2011. Uncoordinated loss of chromatid cohesion is a common outcome of extended metaphase arrest. *PLoS ONE*. 6:e22969. http://dx.doi.org/10.1371/journal.pone.0022969

Théry, M., V. Racine, A. Pépin, M. Piel, Y. Chen, J.B. Sibarita, and M. Bornens. 2005. The extracellular matrix guides the orientation of the cell division axis. *Nat. Cell Biol.* 7:947–953. http://dx.doi.org/10.1038/ncb1307

Toyoshima, F., and E. Nishida. 2007. Integrin-mediated adhesion orients the spindle parallel to the substratum in an EB1- and myosin X-dependent manner. *EMBO J.* 26:1487–1498. http://dx.doi.org/10.1038/sj.emboj.7601599

Toyoshima, F., S. Matsumura, H. Morimoto, M. Mitsushima, and E. Nishida. 2007. PtdIns(3,4,5)P3 regulates spindle orientation in adherent cells. *Dev. Cell*. 13:796–811. http://dx.doi.org/10.1016/j.devcel.2007.10.014

Woodard, G.E., N.N. Huang, H. Cho, T. Miki, G.G. Tall, and J.H. Kehrl. 2010. Ric-8A and Gi alpha recruit LGN, NuMA, and dynein to the cell cortex to help orient the mitotic spindle. *Mol. Cell. Biol.* 30:3519–3530. http://dx.doi.org/10.1128/MCB.00394-10

Wu, C.H., R. Apweiler, A. Bairoch, D.A. Natale, W.C. Barker, B. Boeckmann, S. Ferro, E. Gasteiger, H. Huang, R. Lopez, et al. 2006. The Universal Protein Resource (UniProt): an expanding universe of protein information. *Nucleic Acids Res.* 34(Database issue):D187–D191. http://dx.doi.org/10.1093/nar/gkj161